Protonated Urea Collision-Induced Dissociation. Comparison of Experiments and Chemical Dynamics Simulations

Riccardo Spezia,*,† Jean-Yves Salpin,† Marie-Pierre Gaigeot,† William L. Hase,*,‡ and Kihyung Song*,§

Laboratoire Analyse et Modélisation pour la Biologie et l'Environnement, CNRS UMR 8587, Université d'Evry-Val-d'Essonne, Bd. F. Mitterrand, 91025 Evry Cedex, France, Department of Chemistry & Biochemistry, Texas Tech University, Lubbock, Texas 79409, and Department of Chemistry, Korea National University of Education, Chungbuk, 363-791 South Korea

Received: July 9, 2009; Revised Manuscript Received: September 28, 2009

Quantum mechanical plus molecular mechanical direct chemical dynamics were used, with electrospray tandem mass spectrometry experiments, potential energy surface calculations, and RRKM analyses, to study the gas-phase collision-induced dissociation (CID) of protonated urea. The direct dynamics were able to reproduce some of the experimental observations, in particular the presence of two fragmentation pathways, and, thus, to explain the dynamical origin of the two fragmentation ions observed in the CID spectra. A shattering dissociation mechanism takes place during the collision, and it becomes more important as the collision energy increases, thus explaining the linear increase of the high-energy reaction path (loss of ammonia) versus collision energy. By combining the different theoretical and experimental findings, a complete dynamical picture leading to the fragmentation was identified: (i) Oxygen-protonated urea, the most stable structure in the gas phase, must first isomerize to the nitrogen-protonated form. This can happen by multiple CID collisions or in the electrospray ionization process. (ii) Once the nitrogen-protonated isomer is formed, it can dissociate via two mechanisms: i.e, a slow, almost statistical, process forming a NH_4^+--NHCO intermediate that rapidly dissociates or a fast nonstatistical process which may lead to the high-energy products.

I. Introduction

Collision-induced dissociation (CID) is an important experimental method to study structures, energetics, and kinetics of small molecules,[1−3] clusters,[4−7] and organic[8−10] and biological molecules.[11−14] In CID, an ion is energized by collisions with a rare gas atom or unreactive molecule such as N_2. In the limit of low-energy collisions, electronic excitation is unimportant and the collisions transfer a fraction of the translational energy to vibrational/rotational energy of the molecular ion so that it can eventually dissociate. It is possible to monitor, after CID, the residual parent and product ions.

Fragmentation of the ion may occur by the following two limiting mechanisms: (i) the vibrational energy flows through the ion's modes, and, after intramolecular vibrational energy redistribution (IVR), the ion dissociates; (ii) the collision locally activates one (or few) vibrational mode(s), and fragmentation occurs within one vibrational period. The former model provides a statistical picture that can be described by kinetic models like RRKM theory[15] or phase space theory (PST).[15,16] Mechanism (ii) is a pure dynamical model where the reaction time is much shorter than the IVR time. Such nonstatistical mechanisms were evoked to explain the fragmentation of large molecules, for which statistical models predict fragmentation times so long that fragmentation is not experienced—while there is evidence that these systems dissociate.[17] One nonstatistical mechanism, identified as "shattering",[18,19] occurs in surface-induced dissociation (SID),[20−23] where the projectile ion fragments as it collides with the surface. In contrast, CID is usually thought of as providing statistical dissociation in accord with RRKM theory. However, shattering dissociations and non-RRKM dynamics have been observed in previous experiments[24] and simulations[25] of CH_3SH^+ + Ar CID, experiments[26] and simulations[27] of $CH_3SCH_3^+$ + Ar CID, and simulations[28,29] of $Cr^+(CO)_6$ + Xe and H_2CO^+ + Ne CID. Moreover, it has been suggested from simulations that nonstatistical fragmentation dynamics might also be important for CID of protonated amino acids and peptides.[30,31]

Chemical dynamics simulations[32] can model CID processes by calculating an ensemble of trajectories for which the projectile ion and inert gas collide with a given relative translational energy and all possible relative collision orientations present in CID experiments are sampled.[33] This method, which requires hundreds or thousands of trajectories for statistical relevance, can be done by using an analytic[28] potential energy function or by direct dynamics.[29] For some special cases it is possible to use an analytic function which includes unimolecular decomposition paths for the ion,[28] but more common is to use a molecular mechanical (MM) potential for the ion, which does not describe unimolecular decomposition. The latter yields the efficiency of translation-to-vibration energy transfer in CID.[34] With direct dynamics a quantum mechanical (QM) model is used for the ion, and decompositions which occur during the simulation time length[29] can be studied. *Ab initio* direct dynamics for CID become very computationally expensive as the size of the ion grows, and thus it can be useful to treat only the ion by QM and use MM potentials for interactions with its collision partner.[34]

Urea, the first synthetic organic compound, and its derivatives are of great industrial[36−38] and biomedical[39−42] significance.

* Authors to whom correspondence should be addressed. E-mail: riccardo.spezia@univ-evry.fr (R.S.); bill.hase@ttu.edu (W.H.); ksong@knue.ac.kr (K.S.).

† Université d'Evry-Val-d'Essonne.

‡ Texas Tech University.

§ Korea National University of Education.

10.1021/jp906482v CCC: $40.75
Published on Web 11/03/2009

Since the structure of urea presents key functional groups of larger biomolecules, the reaction dynamics of this model molecule provide some insights into the CID behavior of larger molecules. Urea has been used as a model system in recent experimental and theoretical studies[43,44] of gas-phase divalent cation stability. Protonated urea has been studied in the gas phase using both direct equilibration[45] and Cook's kinetic method,[46] providing experimental thermodynamic stability of the ion and structural information by coupling experiments with computational methods. The neutral species was studied by computational methods by Dixon and Matsuzawa as a model for the study of nonlinear optical properties.[47]

In the work presented here, the gas phase CID of protonated urea was investigated by combining electrospray tandem mass spectrometry (ESI-MS/MS) experiments with electronic structure QM calculations and QM+MM direct chemical dynamics simulations. This latter approach provides useful information regarding fragmentation mechanisms and relationships between the observed fragments (in both the experiments and simulations) and dissociation mechanisms. Protonated urea is a good model system since its potential energy surface (PES) is relatively simple with only two minimum energy structures.[46] The CID simulations were done for both of these structures to investigate the role of the initial structure on the dynamics. RRKM and kinetic analyses of the unimolecular decomposition of protonated urea were performed, based on the PES determined with MP2 theory, to determine the dynamics predicted by statistical theory and compared with those found in the direct dynamics simulations and experiments.

II. Experimental Method

Electrospray MS/MS mass spectra were recorded on a QSTAR PULSAR i (Applied Biosystems/MDS Sciex) hybrid instrument (QqTOF) fitted with a nanospray source. Typically, 6 μL of an aqueous solution of urea (10^{-4} mol L^{-1}) was nanosprayed (20−50 nL/min) using borosilicate emitters (Proxeon). The sample was ionized using a 900 V nanospray needle voltage and the lowest possible nebulizing gas pressure (tens of millibars). The declustering potential DP (also referred to as "cone voltage" in other devices), defined as the difference in potentials between the orifice plate and the skimmer (grounded), ranged from 0 to 60 V. The operating pressure of the curtain gas (N_2) was adjusted to 0.7 bar by means of pressure sensors, as a fraction of the N_2 inlet pressure. To improve ion transmission and subsequent sensitivity during the experiments, the collision gas (CAD, N_2) was present at all times for collisional focusing in both the Q0 (ion guide preceding the quadrupole Q1 and located just after the skimmer) and Q2 (collision cell) sectors. Protonated urea was mass-selected using Q1 and allowed to collide with N_2 at various collision energies ranging from 8 to 30 eV in the laboratory frame (the collision energy is given by the difference between the Q0 and Q2 potentials). The resulting fragments were separated by a time-of-flight (TOF) analyzer after orthogonal injection. Low gas pressures (typically 1−2 10^{-5} mbar) were used to limit multiple ion−molecule collisions. Urea was purchased from Aldrich (St. Quentin-Fallavier, France) and was used without further purification. All the measurements presented hereafter were carried out in 100% water purified with a Milli-Q water purification system.

III. Computational Details

A. Geometry Optimizations and RRKM Analyses. Geometry optimizations of minima and saddle points on the protonated urea potential energy surface (PES) were performed using MP2 with the 6-31G* basis set and the much larger aug-cc-pVTZ basis set, which serves as a reference. Energies of the fragmentation products were calculated at both levels of theory. Vibrational frequencies for all stationary points were calculated with both basis sets and used in the RRKM calculations. These calculations were performed using Gaussian03.[48]

RRKM theory[15] was used to obtain microcanonical rate constants for protonated urea isomerizations, using the standard expression

$$k(E) = \frac{\sigma N^{\#}(E - E_0)}{h\rho(E)} \quad (1)$$

where σ is the reaction path degeneracy, $N^{\#}(E - E_0)$ is the sum of states at the transition state (TS), $\rho(E)$ is the reactant's density of states, and h is Planck's constant. The TSs are located at saddle points on the PES. The sum and density of states were calculated from vibrational frequencies using the direct count algorithm, as implemented in the RRKM code developed by Zhu and Hase.[49]

Rate constants obtained by RRKM or PST were used to perform a kinetic analysis using the vibrational and rotational energy transfer probabilities obtained from nonreactive trajectories. Thus, the probability of the two fragmentation pathways were calculated (as done in ref 50) for $t = 2.5$ ps, which is the "time limit" of the dynamics.

B. Potential Energy Function for CID Simulations. The potential energy function for the collision system, consisting of protonated urea (urea-H^+) and the projectile (Ar), is written as

$$V = V_{\text{urea}} + V_{\text{Ar-urea}} \quad (2)$$

where V_{urea} is the intramolecular potential energy of urea-H^+ and $V_{\text{Ar-urea}}$ is the Ar/urea-H^+ intermolecular potential. The intramolecular potential energy, V_{urea}, was obtained from MP2/6-31G* calculations, which represents the isomerization and dissociation pathways of urea-H^+. The intermolecular potential is expressed as a sum of two-body terms between Ar and the atoms of urea-H^+, with each two-body term given by

$$V_{\text{Ar-urea}} = a\exp(-br) + \frac{c}{r^9} \quad (3)$$

This potential is purely repulsive—c is always positive—and was developed to simulate CID of protonated peptides.[51] The same parameters (Table 1) were used as reported in this earlier study. The use of a purely repulsive potential is justified by the

TABLE 1: Intermolecular Potential Energy Parameters for Urea-H^+ + Ar[a]

potential	*a*	*b*	*c*
ArC	8471.329	4.648228	304.6066
ArH (NH)	4220.855	2.982401	3.719138
ArO	12914.72	2.681826	99.56698
ArO (OH)	15387.06	2.698321	90.09528
ArN (sp2)	8186.600	2.328971	218.8906
ArN (sp3)	13609.85	2.433643	101.5290
ArH(OH)	8696.623	4.196012	304.6066

[a] Parameters from ref 51. Units are kcal/mol, $Å^{-1}$, and kcal $Å^9$/mol for *a, b,* and *c*, respectively.

fact that the potential energy minimum between Ar and urea-H^+ is small, with respect to the collision energies considered here. In addition, the key feature to consider in CID simulations is the short-range repulsion which is responsible for energy transfer and ensuing projectile ion fragmentation.

C. Direct Dynamics Trajectory Simulations. Two urea-H^+ structures were considered for the direct dynamics simulations: one protonated on oxygen (OPr) and one on nitrogen (NPr), with their geometries optimized at the MP2/6-31G* level of theory. As discussed below, the potential energy minimum of NPr, calculated with MP2 and the 6-31G* and aug-cc-pVTZ basis sets, is 9.7 and 13.8 kcal/mol higher in energy, respectively, than that for OPr. Thus, for thermal conditions there is negligible population of the NPr isomer. However, ESI experiments are likely to be nonthermal for small systems. Several reports have demonstrated that isomerization of ions can take place during the ESI process,[52−54] and internal proton transfer previous to decomposition starting from a protonated carbonyl compound was also observed.[55] Consequently, there may be a substantial population of NPr. Thus, for the work presented here, collisions with both OPr and NPr were investigated in the direct dynamics simulations. A model 300 K temperature was used for each isomer.

Initial conditions for each urea-H^+ isomer were chosen by adding a quasi-classical 300 K Boltzmann distribution of vibrational/rotational energies about the isomers' potential energy minima.[56−58] Energies for the normal modes of vibration were selected from a 300 K Boltzmann distribution. The resulting normal mode energies were partitioned between kinetic and potential energies by choosing a random phase for each normal mode. A 300 K rotational energy of RT/2 was added to each principal axis of rotation for the isomers. Vibrational and rotational energies were transformed into Cartesian coordinates and momenta following well-known algorithms implemented in VENUS.[59,60] The isomer was then randomly rotated about its Euler angles to take into account the random directions of the Ar + urea-H^+ collisions. Relative velocities were then added to Ar + urea-H^+ in accord with the center-of-mass collision energy and impact parameter. Collision energies of 101.5, 130.5, and 145.1 kcal/mol were considered, corresponding to laboratory frame energies of 14, 18, and 20 eV, respectively. The impact parameter, b, was chosen randomly between 0 and b_{max}. The latter was fixed to the value of 3.0 Å from geometrical considerations and the finding that collisions with larger values of b did not transfer sufficient energy to fragment urea-H^+. This value was reduced to 2.5 Å for the OPr simulations since, as shown in the results section, no fragmentations were observed in the CID simulations using OPr as the starting structure.

The trajectories were calculated using a software package consisting of the general chemical dynamics computer program VENUS96[59,60] coupled to Gaussian03.[48] The latter was used to calculate the potential energy and gradient for the urea-H^+ intramolecular potential. The classical equations of motion were integrated using the velocity Verlet algorithm[61] with a time step of 0.2 fs that gives energy conservation for both reactive and nonreactive trajectories. The trajectories were initiated at an ion−projectile distance of 7.0 Å, large enough to guarantee no interaction between the ion and the colliding atom, and halted at a distance of 100 Å to allow substantial intramolecular motion of the urea-H^+ ion. This corresponds to a total integration time of ~2.5 ps. A trajectory was also stopped if the ion dissociates. In that case, the criterion distance of 7.0 Å was also used to guarantee no interactions between fragments. For each simulation, identified by the collision energy and urea-H^+ isomer, approximately 250 trajectories were calculated.

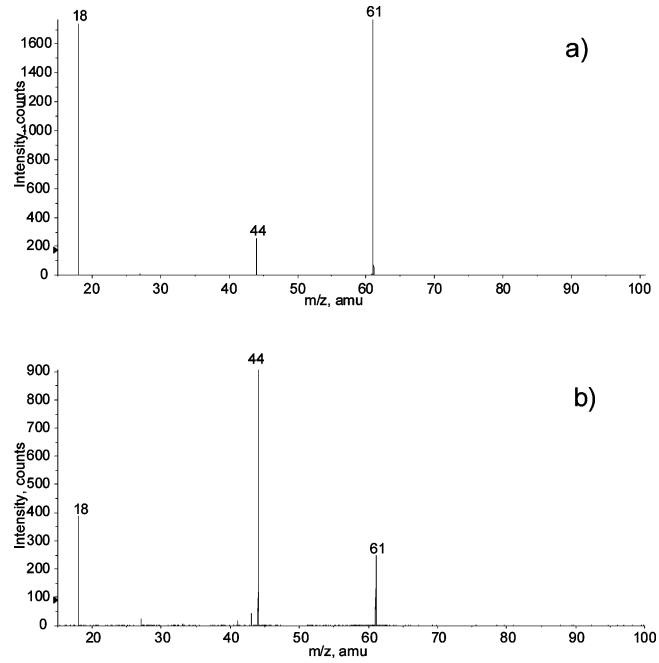

Figure 1. MS/MS spectra of protonated urea recorded at a collision energy of 20 eV (laboratory frame) for a (a) 15−180 and (b) 15−100 mass range chosen for quadrupole transmission.

IV. Results and Discussions

A. Mass Spectrometry and CID Experiments. The nano-electrospray spectrum (not shown) of an aqueous solution of urea is particularly simple as it exhibits only three significant peaks at m/z of 61, 83, and 121. The former, which is clearly overwhelming, corresponds to protonated urea and the latter to a protonated urea dimer as confirmed by its MS/MS spectrum (loss of 60 Da corresponding to one urea molecule). The protonated dimer is observed under mild source/interface conditions (typically with a cone voltage set to 0−10 V), and its abundance rapidly decreases as this voltage is increased. The peak at $m/z = 83$ corresponds to an adduct of urea with residual sodium.

Protonated urea was mass-selected by the first quadrupole and then allowed to collide with N_2 in the Linac collision cell (Q2). A typical MS/MS spectrum is given in Figure 1. Two dissociation channels are observed, giving rise to ammonium ions NH_4^+ ($m/z = 18$) and a $m/z = 44$ species associated with the loss of ammonia. These channels correspond to

$$\text{path 1:} \quad \text{urea-H}^+ \rightarrow \text{NH}_3 + \text{CONH}_2^+$$

$$\text{path 2:} \quad \text{urea-H}^+ \rightarrow \text{NH}_4^+ + \text{OCNH}$$

The MS/MS spectra are very likely obtained under a multiple-collision regime. With the CAD parameter (which controls the amount of N_2 introduced into Q2) set to its minimum value, the pressure value measured by the ion gauge, located near the vicinity of Q2, is about 2×10^{-5} torr. But, according to several reports, the actual pressure inside Q2 is closer to 10^{-2} torr.[62] Given the length and the internal diameter of Q2 (22 and 4.1 cm, respectively), the mean free path for a moving N_2 molecule, according to the gas kinetic theory, is roughly 5 mm at 10^{-2} torr. So a molecule of N_2 may undergo tens (up to 40) of

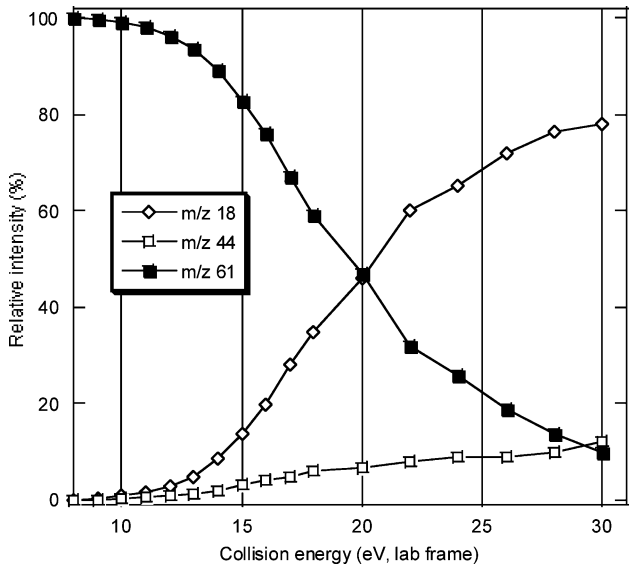

Figure 2. Intensity of precursor and fragment ions generated upon CID of protonated urea (for the 15−180 mass range quadrupole transmission).

collisions within Q2. This is a lower limit for the urea-H^+ ions of interest which have a larger diameter and, thus, a larger collision cross section.

In order to check the effect of the collision energy on the branching ratio, the collision energy was varied from 8 to 30 eV in the laboratory frame (Figure 2). This corresponds to center of mass collision energies ranging from 2.3 to 8.5 eV. It was found that 8 eV (E_{lab}) is the smallest value of the collision energy for which a sufficient amount of fragment ions could reach the detector after orthogonal injection in the TOF. However, at 8 eV, no fragmentation occurred. The lowest collision energy for which fragmentation was observed is 9 eV.

As illustrated in Figure 2, the formation of ammonium ions, path 2, dominates whatever the collision energy. It is worth noting that the observation of ammonium ions is not straightforward. Similar experiments carried out on a triple quadrupole instrument resulted in the observation of $m/z = 44$ ions, path 1,[63] but a surprisingly small amount of ammonium ions. On the other hand, observation of ammonium ions on the QSTAR was possible but strongly dependent on two interdependent parameters: i.e., the frequency of the orthogonal injection pulse and the chosen mass range which controls the way that ions are transferred through the first and second quadrupoles. Ions are indeed usually passed through Q1 and Q2 in several "hops" over the chosen mass range. Each hop consists of a chosen m/z, which in turn corresponds to a selected radiofrequency. At that particular value, quadrupoles transmit for a well-defined time (50% of the scan time when 2 m/z are chosen, 33% for 3 m/z, and so on) all the ions from 80% to fivefold the chosen m/z. Consequently, changing the mass range can have dramatic effects on the abundance of ions observed in both the MS and MS/MS spectra as illustrated by Figure 1a, b. QqTOF instruments are known for discriminating low mass ranges and are not designed to study very small ions such as NH_4^+ and urea-H^+. One needs to pay attention to the way ions are transferred within Q1 and Q2 in order not to lose ions due to improper transmission.

B. Potential Energy Surface and RRKM Analyses. Either the oxygen or nitrogen of urea may be protonated, providing two isomers, oxygen-protonated (OPr) and nitrogen-protonated (NPr). OPr is known to be more stable in the gas phase.[46] MP2

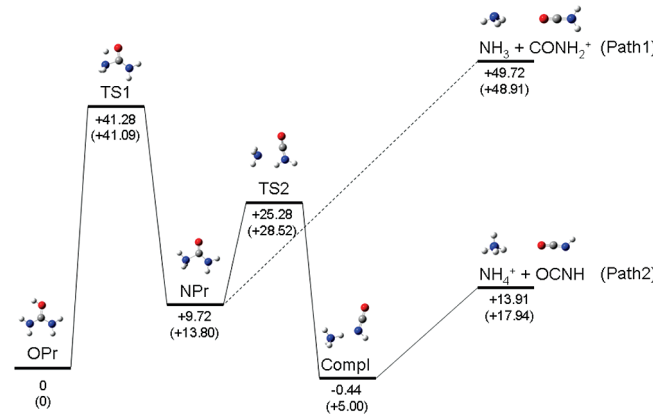

Figure 3. Potential energy profile for the dissociation of the two protonated urea isomers, OPr and NPr. There are two dissociation pathways. Energies are in kcal/mol, calculated at the MP2/6-31G* and MP2/aug-cc-pVTZ (in parentheses) levels of theory. Optimized structures are also shown. Oxygen is red, nitrogen blue, carbon gray, and hydrogen white.

calculations give the same result, with both the 6-31G* and MP2/aug-cc-pVTZ basis sets, as shown in Figure 3. This figure also gives energies for all the stationary points found from the MP2 calculations. There are three minima, connected by two TSs, and two fragmentation channels. The potential energy curve in Figure 3 has important features that are useful to understand and rationalize the observed CID dynamics. First, OPr can isomerize to NPr via a proton transfer TS which has a barrier of ∼41 kcal/mol. This proton transfer is necessary to obtain subsequent fragments that cannot be obtained—at least in a static picture—directly from the most stable minimum, OPr. The direct chemical dynamics simulations of CID, starting with OPr, can shed light on this aspect. The NPr structure is a key structure to produce both experimentally observed fragments, i.e., NH_4^+, m/z 18, and $CONH_2^+$, m/z 44.

Finally, there is a third minimum, called "Compl", which has almost the same potential energy as the most stable isomer OPr. This intermediate is a NH_4^+--NHCO complex (structure in Figure 3), from which it is possible to form the more stable fragments NH_4^+ + OCNH (path 2) from NPr via TS2. On the other hand, the high-energy fragments NH_3 + $CONH_2^+$ (path 1) are directly linked to NPr and produced by the direct loss of NH_3. Thus, a direct dynamics simulation of CID, with NPr as the starting structure, can determine if it is possible to form both sets of fragments from this isomer.

It is also of interest to investigate the RRKM rate constants for the isomerizations OPr ↔ NPr and NPr → Compl. The rate constants for the OPr ↔ NPr isomerizations, as obtained from MP2/6-31G* and MP2/aug-cc-pVTZ energies and frequencies, are shown in Figure 4. These isomerizations occur on a 10−1000 ps time scale, at the collision energies of the CID experiments, and thus statistical theory predicts that they should be unimportant for the 2.5 ps time scale of the direct dynamics simulations (as discussed below, on average ∼50% of the collision energy is transferred to internal degrees of freedom of urea-H^+). Figure 5 gives the RRKM rate constants for the NPr → Compl reaction, which leads to the path 2 fragments. These rate constants are much larger than those in Figure 4, and statistical theory predicts that the NPr → Compl reaction should be observed during the 2.5 ps direct dynamics simulations. Of interest is the actual dynamics observed in the simulations, including possible nonstatistical effects.

As discussed below, a substantial amount of rotational energy is transferred to the urea-H^+ isomers in their collisions with

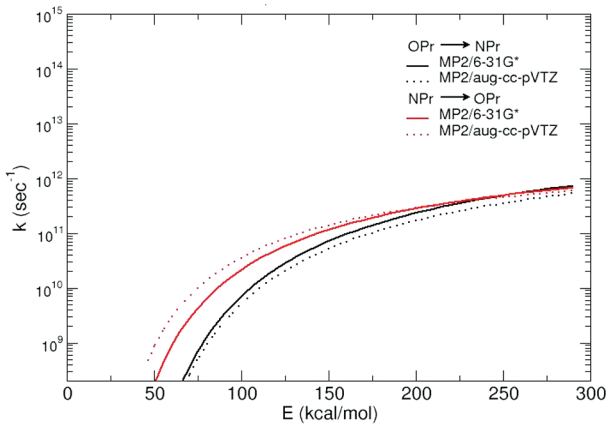

Figure 4. RRKM rate constants versus vibrational energy for OPr → NPr (black curves) and NPr → OPr (red curves) isomerization. Solid lines, MP2/6-31G* PES; dotted lines, MP2/aug-cc-pVTZ PES. There is no rotational energy.

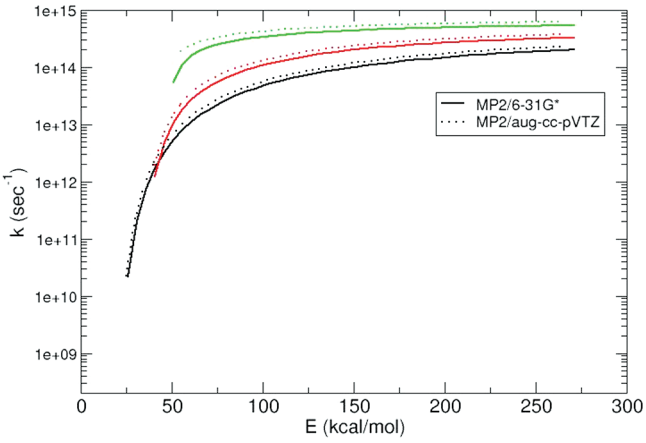

Figure 5. RRKM rate constants for the NPr → Compl reaction versus vibrationl energy for different total rotational energies. Solid line, MP2/6-31G* PES; dashed line, MP2/aug-cc-pVTZ PES. Different rotational energies are added: 10 kcal/mol (in black), 30 kcal/mol (in red), and 50 kcal/mol (in green). The same rotational energy is added to each rotational axis: i.e., for a total rotational energy of 30 kcal/mol, 10 kcal/mol is added to each rotational axis.

Ar. This energy has a negligible effect on the OPr ↔ NPr isomerizations, but does affect the NPr → Compl isomerization. TS1, which mediates the OPr ↔ NPr isomerizations, has a heavy-atom equilibrium geometry very similar to those for OPr and NPr. Thus, the TS1 moments of inertia are nearly the same as those for OPr and NPr, and rotational excitation does not have a significant effect on the OPr ↔ NPr isomerization rate constants.[15] In contrast, the moments of inertia for TS2 are larger than those for NPr, and rotational excitation increases the NPr → Compl rate constant as shown in Figure 5.

C. Direct Dynamics Simulations. ***1. Efficiency of Energy Transfer.*** Direct chemical dynamics simulations, of collisions between Ar and both urea-H^+ isomers, were performed for 101.5, 130.5, and 145.1 kcal/mol relative collision energies, to study the effects of low, medium, and high collision energies. Figure 6 shows the resulting average energy transfer to the internal degrees of freedom of both isomers versus impact parameter *b*. Energy transfer is similar for both isomers, with a somewhat higher efficiency to NPr. It is nearly constant over a broad range of *b* and then gently decreases as *b* increases. For small $b \rightarrow 0$, the energy transfer efficiency also decreases. The maximum is approximately 50% of the collision energy.

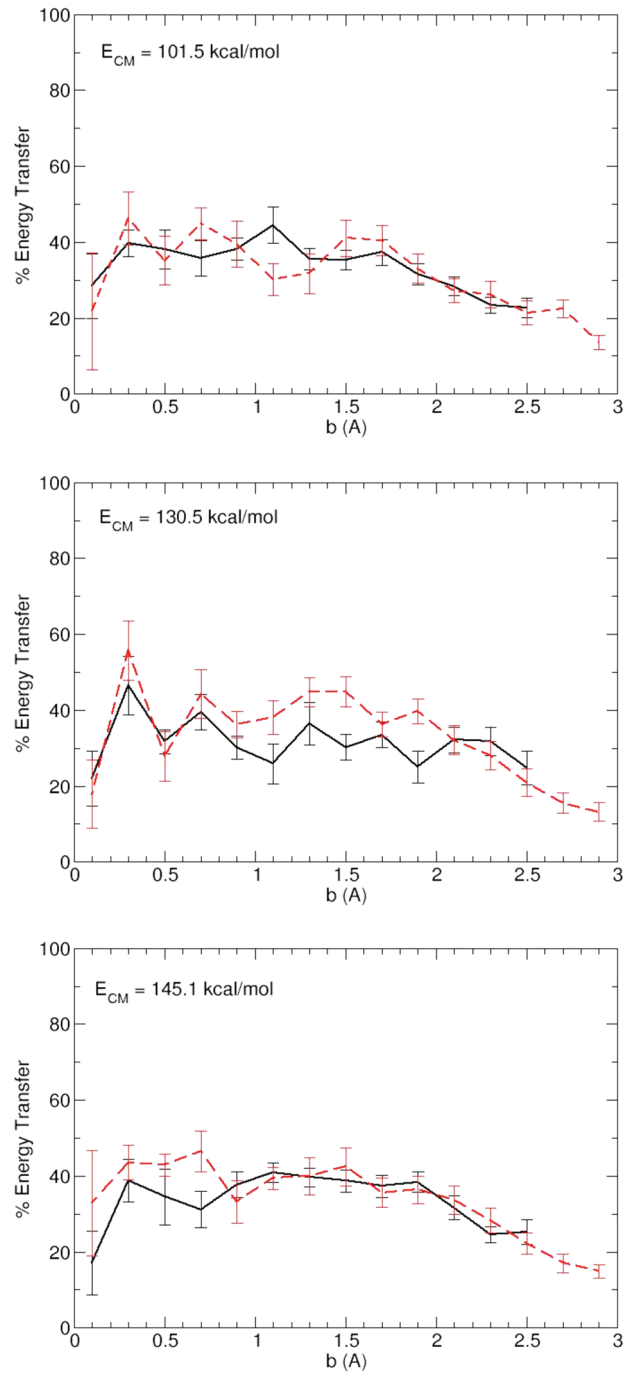

Figure 6. Percentage energy transfer to the internal degrees of freedom (vibration + rotation) of the two urea-H^+ isomers versus impact parameter for the three collision energies: OPr, solid line; NPr, dashed line. Uncertainties are standard deviation of the means.

Energy transfer to urea-H^+ includes both vibration and rotation, and their individual transfers are shown in Figure 7 for the OPr isomer. Similar results (not shown) are found for the NPr isomer. At small *b*, less than 0.5 Å, energy transfer to vibration dominates, but for larger *b* energy transfer to rotation is more important. For $b = 0$, the collision is with the urea-H^+ center of mass and has no orbital angular momentum, and energy transfer to rotation becomes inefficient. At the larger *b*, energy transfer to rotation is approximately a factor of 2 larger than that to vibration. Since the probability of a collision with *b* is proportional to *b*, energy transfer to rotation is much more important than to vibration. Averaging the results in Figure 7 over *b* gives approximate percentages of energy transfer to

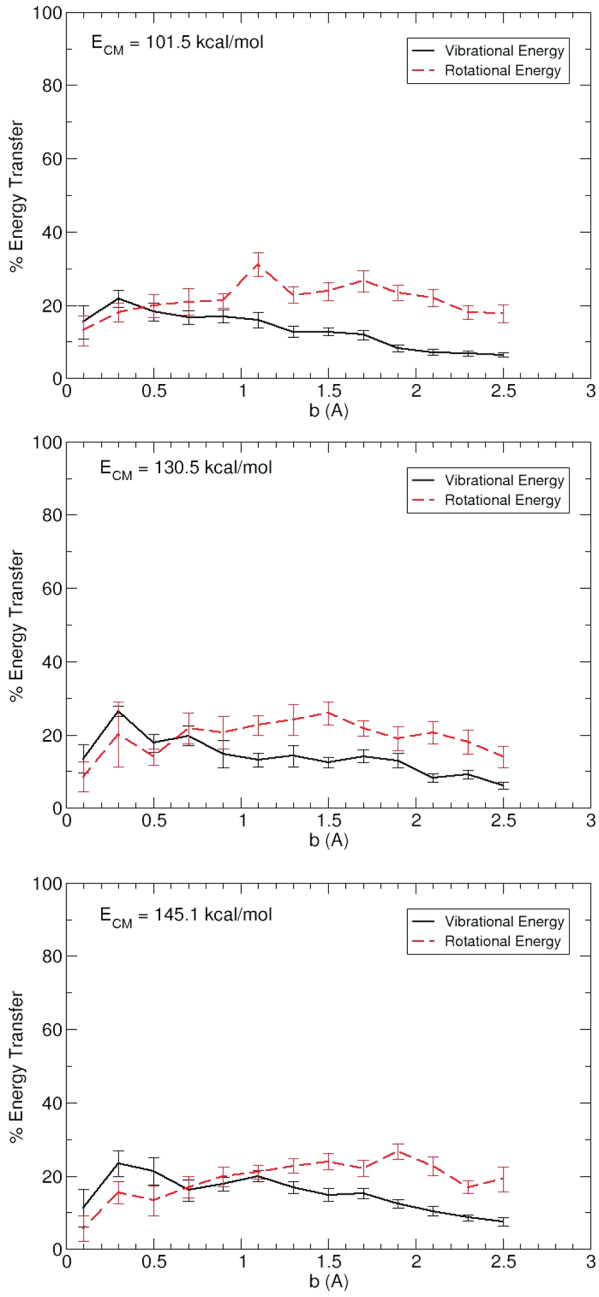

Figure 7. Percentage of collisional energy transfer to vibrational and rotational degrees of freedom of OPr versus impact parameter for different collision energies.

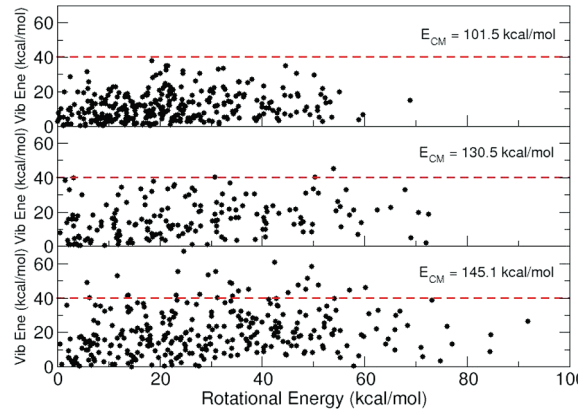

Figure 8. Scattering plot of rotational versus vibrational energy distributions obtained from nonreactive OPr trajectories for the three collision energies. The horizontal line identifies the barrier to reach TS1.

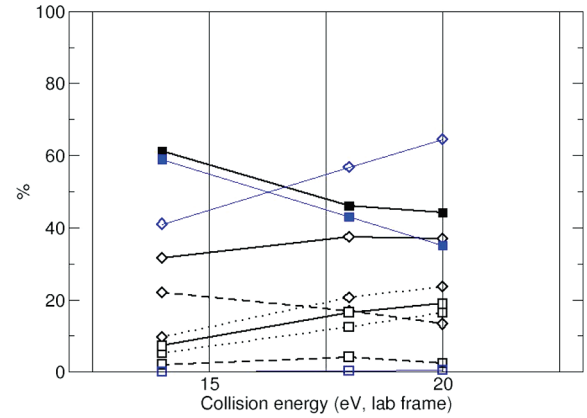

Figure 9. Percentages of remaining NPr reactant (■), $NH_3 + CONH_2^+$ products for path 1 (□), and $NH_4^+ + OCNH$ products for path 2 (◇), for the three collision energies. Total percentage, (—); ET percentage, (---); shattering percentage, (•••). In blue we show results obtained from kinetic analysis.

rotation of 22, 20, and 21% for the 101.5, 130.5, and 145.1 kcal/mol collision energies, respectively, while the respective energy transfers to vibration are 11, 12, and 14%. The percentage energy transfers are not strongly dependent on the collision energy, particularly for rotation. Efficient energy transfer to projectile ion rotation has also been found in previous simulations of CID, and this efficiency depends on the projectile's structure.[64,65] Energy transfer to rotation is more probable for ions with anistropic, nonspherical-like structures, and the current results for Ar + urea-H^+ are consistent with these previous findings.

To interpret the urea-H^+ fragmentation dynamics, and also to apply RRKM theory, it is important to know the correlation between urea-H^+ vibrational and rotational excitation. This is illustrated by the scatter plots in Figure 8 for OPr excitation at the different collision energies. There is not a strong correlation between the vibrational and rotational energy transfer. However, for the largest rotational energy transfers, there is a small anticorrelation between the vibrational and rotational excitations; i.e., for a large rotational excitation, the vibrational excitation tends to be small.

2. Fragmentation Dynamics. While energy transfer is very similar for the two isomers, their ensuing unimolecular dynamics are much different. With OPr as the starting structure, no isomerizations or fragmentations were observed at either of the three collision energies investigated. This is in agreement with the RRKM rate constants in Figure 4, which say that isomerization to NPr only occurs on time scales longer than the 2.5 ps time scale of the simulations. No reaction channels are available to OPr for the simulation time scale.

In contrast, for the NPr simulations fragmentation occurs via both reaction channels. Figure 9 shows the probabilities of forming the path 1 and path 2 fragmentation products and the percentage of the initial urea-H^+ ion remaining at the end of the simulation, for the three collision energies studied. Very good qualitative agreement is found with the experimental results reported in Figure 2. In particular, the decrease in the parent ion intensity (m/z = 61) is very similar for the experiments and simulations, reaching 50% for both at 20 eV. The increase of the fragmentation products versus collision energy is also similar for the experiments and simulations. There is a linear increase of the m/z = 44 ion population, corresponding

TABLE 2: Percentages of Different Trajectory Types and Their Average Lifetimes To Form Fragmentation Products for NPr CID[a]

	%			<time>		
	CE = 101.5	CE = 130.5	CE = 145.1	CE = 101.5	CE = 130.5	CE = 145.1
no reaction	61.2	46.09	44.18			
path 1/shattering	5.2	12.35	16.46	540.3	345.4	353.9
path 1/ET	2.0	4.12	2.41	902.0	1119.6	721.7
path 2/shattering	9.6	20.58	23.69	697.1	624.2	548.5
path 2/ET	22.0	16.87	13.25	1245.3	1120.0	944.9

[a] CE is the collision energy, and ET is the energy transfer fragmentation mechanism. CE is in kcal/mol, and time is in fs.

to path 1, and the $m/z = 18$ ion intensity first increases with collision energy and then reaches a plateau. The relative intensity of the two fragmentation ions may be strongly affected by the experimental transmission/detection setup, and thus, a full quantitative comparison between the experiments and simulations is not possible.

An important contribution from the simulations is an atomic-level description of the fragmentation dynamics. As described in the Introduction, it is possible to define two different fragmentation mechanisms: (i) *shattering* and (ii) *energy transfer* (ET). The reactive trajectories are categorized by whether dissociation occurred by shattering or ET. Figure 9 and Table 2 give the percentages of the NPr trajectories fragmenting via ET and shattering versus the collision energy, for both path 1 and path 2. It is seen that the path 1 products are primarily formed by shattering. This implies that to form these products, instead of the much lower energy path 2 products, requires the nonstatistical shattering mechanism in which the collision deposits energy into $NH_3 + CONH_2^+$ relative motion leading to direct dissociation without IVR. Only a very small fraction of the $NH_3 + CONH_2^+$ fragmentation occurs by the ET mechanism. The linear increase in the probability of path 1 shattering versus collision energy is consistent with more probable initial localization of energy in $NH_3 + CONH_2^+$ relative motion with increase in the collision energy. A similar effect is seen in surface-induced dissociation (SID).[66,67]

In contrast, the path 2 products are formed by both the shattering and ET mechanisms. The probability of shattering increases, and the probability of ET fragmentation decreases, with increase in collision energy. The combination of these two effects gives rise to the observed plateau for the probability of path 2 in the simulations. In experiments this plateau is observed (i.e., $m/z = 18$ in Figure 2) for higher collision energies than in the simulations. This difference is probably due to the fact that the simulations underestimate—as shown in the next section—the formation of path 2 products via the ET mechanism. Thus, the plateau arising from a balance between the shattering and ET mechanisms is found at lower collision energies in the simulations.

Dissociation of NPr via the ET mechanism occurs within the 2.5 ps time scale of the direct dynamics simulations, which is the same time scale as predicted by RRKM theory for NPr to cross the rate-controlling TS2 (Figure 5) leading to path 2. Figure 10 gives the time-dependent probabilities of forming the path 1 and path 2 products and for reactant ions remaining, for the different collision energies. The path 2 products dominate at each collision energy, with the path 1 products becoming more important with increase in collision energy. The path 1 products are formed at shorter times as compared to those for path 2. This is a result of the importance of shattering for path 1. With increasing collision energy, the path 2 products are obtained in shorter times because of faster ET dissociation and an increasing importance of shattering.

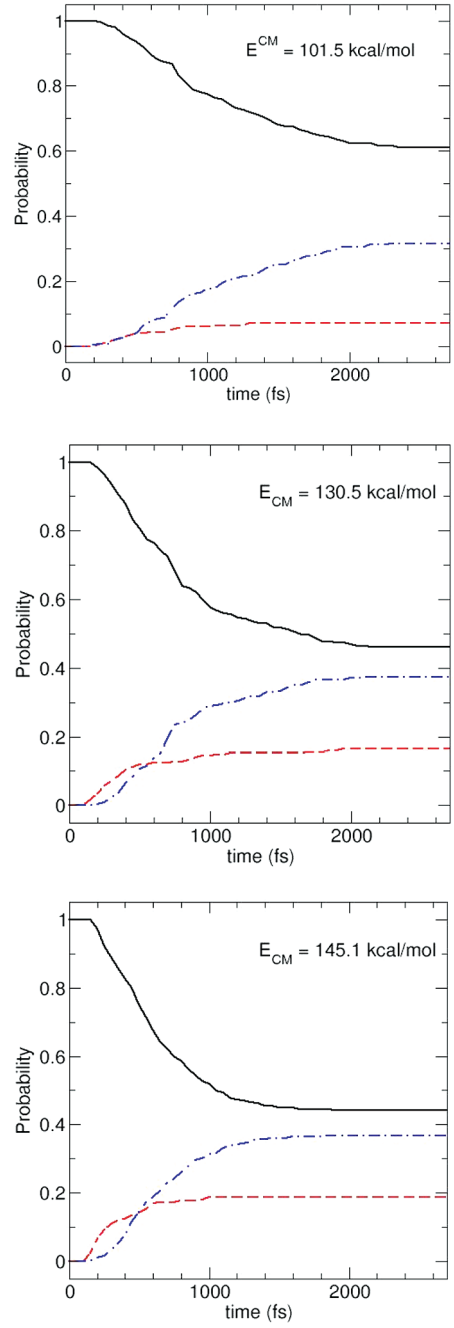

Figure 10. Probabilities of forming path 1 products (---), path 2 products (-•-•-), and NPr reactant (—) versus time. Results are given for each of the three collision energies.

It is interesting to note that the trajectories taking the high-energy path 1 reaction channel proceed faster as compared to the low-energy path 2 channel. This is due to the fact that path 2 is obtained via both a fast shattering and a slow ET

mechanism, while path 1 is mainly reached via fast shattering. Furthermore, the shattering mechanism leading to path 1 products is faster than the shattering mechanism leading to path 2 products.

Table 2 gives the average times needed to obtain the path 1 and path 2 products with NPr as the projectile ion. These times are given as a function of the fragmentation mechanism, i.e., shattering or ET, and the collision energy. To assist in interpreting these times, it is useful to consider the different atomic-level dynamics for the dissociation paths. Ammonia for path 1 can be obtained by a sudden elongation of one C−N bond, while forming NH_4^+ for path 2 requires proton transfer in addition to C−N bond rupture. If C−N elongation is not sufficient to directly form the $NH_3 + CONH_2^+$ products, the $NH_4^+ +$ OCNH products may be formed via either shattering or ET. The former mechanism proceeds as discussed above, while ET may happen in two ways. First, elongation of the C−N bond may be sufficiently slow so that the leaving NH_3 has enough time to attach the proton, forming NH_4^+ and taking the path 2 low-energy channel. In agreement with these dynamics is the very small probability of the ET mechanism for path 1. Second, ET may occur via formation of a NH_4^+--NHCO complex that is similar to the Compl structure of Figure 3. With its excess energy, this complex quickly dissociates forming the path 2 products. None of these complexes survive at the end of the simulations.

For the MP2/6-31G* level of theory used for the direct dynamics simulations, the OPr → NPr isomerization barrier of TS1 is 41.3 kcal/mol and the barrier for NPr → $NH_3 + CONH_2^+$ dissociation, path 1, is nearly the same and 40.0 kcal/mol (see Figure 3). Thus, simply based on these energetics, it may seem surprising that NPr dissociates via path 1, while OPr → NPr isomerization does not occur. The origin of this difference is tied to the large rotational excitation of the urea-H^+ isomers. As discussed above in section IV.B, rotational excitation does not promote OPr → NPr isomerization since the TS1 moments of inertia are nearly the same as those for OPr. On the contrary, rotational excitation of NPr facilitates path 1 since the dissociating system's moments of inertia increase, with two approaching infinity as the C−N bond ruptures and the fragments separate. These dynamics transfer rotational to vibrational energy, thus enhancing path 1. The statistical modeling of this effect is treated by variational RRKM theory,[15] and such RRKM calculations are important for future studies.

3. Nonreactive Urea-H$^+$ Ions. There is a nonnegligible amount of urea-H^+ ions (i.e., ∼50% for the NPr starting structure, see Table 2, and 100% for OPr) which are vibrationally/rotationally excited but do not isomerize or dissociate during the 2.5 ps time scale of the simulations. The vibrational and rotational energy distributions of these ions are shown in Figures 11 and 12 for the NPr and OPr starting structures, respectively. Most of the nonreactive NPr ions have low vibrational energies and an insufficient amount to reach the path 1 products, as shown by the vertical line at 40 kcal/mol. More ions have sufficient vibrational energy to reach TS2 (the vertical line at 15.56 kcal/mol) and form the path 2 products, but the fraction is still small. After 2.5 ps of internal vibrational dynamics and IVR, it is likely that decomposition of these ions is statistical, and thus, even if they contain sufficient energy to follow path 1, they will follow path 2. Thus, an excellent model is one that assumes ions with vibrational energy in excess of the TS2 barrier will form the path 2 products, increasing the population of path 2 and giving better agreement with experiment (Figures 2 and 9).

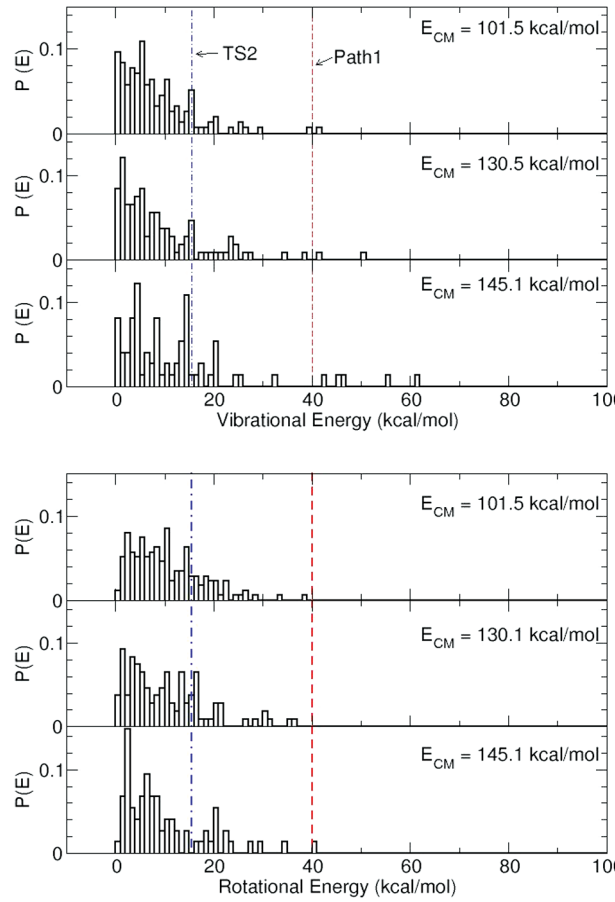

Figure 11. Nonreactive NPr trajectories' vibrational and rotational energy distributions for the three collision energies. The vertical lines identify the barriers to reach TS2 and the path 1 products from NPr. As discussed in the text, rotational energy can assist crossing TS1 and reaching the path 1 products.

From Figure 11 it is found that the percentage of nonreactive trajectories that have enough vibrational energy to pass the TS2 barrier, thus forming path 2 products, is 16, 22, and 28% for the 101.5, 130.1, and 145.1 collision energies, respectively. Rotational energy can also assist the formation of Compl via TS2 (see Figure 5), thus augmenting the population of path 2 products and giving even better agreement with experiments. Looking for principal axes of inertia of TS2 and Compl structures, we note that one axis is almost parallel to the breaking C−N bond, so that rotational energy on that axis will not contribute to dissociation. Assuming the approximation that rotational energy is equally distributed, we can quantify the internal energy of nonreactive NPr trajectories as $E_{int} = E_{vib} + 2/3\ E_{rot}$. In Figure 13 we show the E_{int} distribution from which we can calculate the percentage of nonreactive trajectories with enough energy to pass the TS2 barrier, thus forming path 2 products, finding 39, 52 and 63% for the 101.5, 130.1, and 145.1 collision energies, respectively.

Using the vibrational and rotational energy distributions, obtained from nonreactive NPr trajectories, we performed a kinetic analysis using RRKM theory (for path 2) and PST (for path 1) rate constants; i.e. as above it was assumed that the rotational energy is equally distributed between the three rotational axes so that $E_{int} = E_{vib} + 2/3\ E_{rot}$ is available for transfer to vibration. In Figure 9 we show the probability of following path 1, path 2, and the parent ion ($m/z = 61$) as a function of collision energy, and we compare these results with the simulations. Note that the path 1 products have a very small

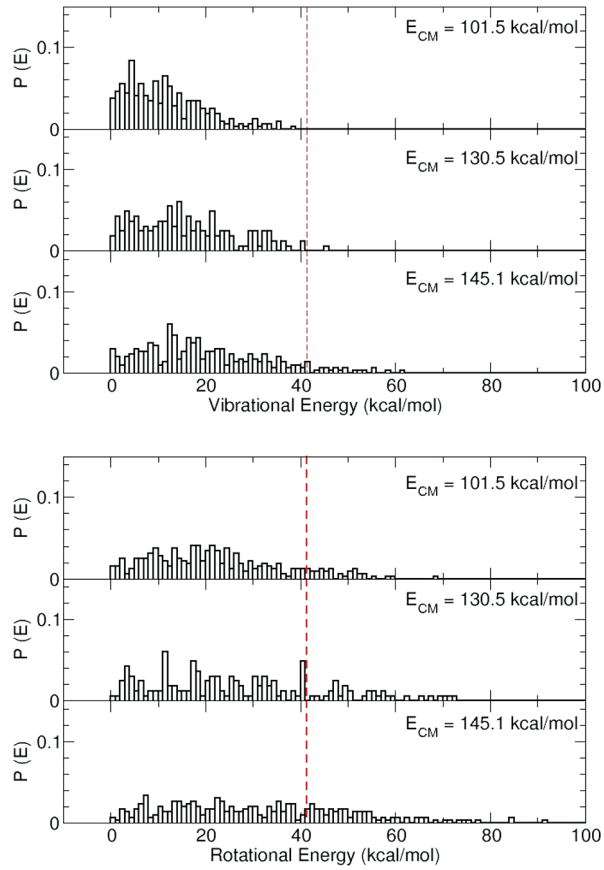

Figure 12. Nonreactive OPr trajectories' vibrational and rotational energy distributions for the three collision energies. The vertical line, for the vibrational distributions, identifies the barrier to reach TS1. As discussed in the text, rotational energy is expected to provide negligible assistance in crossing TS1.

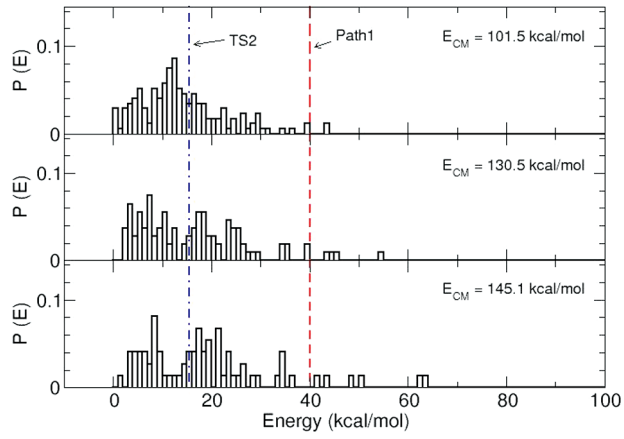

Figure 13. Nonreactive NPr trajectories' internal energy ($E_{int} = E_{vib} + 2/3\ E_{rot}$) distributions for the three collision energies. The vertical lines identify the barriers to reach TS2 and the path 1 products from NPr.

probability, even smaller than the ET simulation results. This is quite expected since the ET dynamics do not involve full IVR as assumed by the statistical approach. On the other hand, the kinetic analysis overestimates the path 2 probability for both the simulations and experiments (see also Figure 2). Finally, good agreement was found for the yield of the parent ion, arising from a compensation between over- and underestimations of path 2 and path 1 probabilities.

Figure 12 gives the same analysis as above, but for the OPr trajectories. The critical barrier here is the one for TS1, yielding OPr → NPr isomerization. At the lowest collision energies there are no ions with sufficient energy to reach the TS1 barrier. For the 130.5 and 145.1 collision energies, 2 and 9% of the OPr molecules have sufficient energy to pass TS1. For this reaction, rotational energy does not have an important role in crossing the TS1 barrier. However, as discussed above, multiple collisions are possible in the experiments. Thus, these ions may acquire the needed energy to cross the TS1 barrier by successive collisions. This isomerization is expected to occur on a longer time scale, and RRKM theory predicts the resulting NPr ions will preferentially form the path 2 products.

V. Conclusions

In this work we have studied the collision-induced dissociation of protonated urea in the gas phase combining experimental ESI-MS/MS studies with direct chemical dynamics. A QM+MM approach was employed, which is able to catch key features of experimental results. In particular we noticed that even for a system that has a simple PES and a simple CID spectrum, the rationalization of the fragmentation pathways is not straightforward. The statistical unimolecular dissociation theory mainly seems to hold for high-barrier cases and for low-collision energies. In fact, direct dynamics results have shown that the shattering mechanism is important also for CID and the probability of having such nonstatistical dynamics increases as the collision energy increases. Moreover, this mechanism is responsible for the formation of high-energy products (ammonia loss) that cannot be formed by a slow statistical dynamics because in that case the low-energy dissociation channel (path 2) has time to be opened. Note that the high-energy path ion (*m*/*z* 44) was found also in experiments. In addition, the direct dynamics chemical simulations were able to find and explain the physical basis of the presence of this ion, while statistical calculations underestimate the probability of forming this ion in the time length of the simulations.

Another important aspect pointed out by the dynamics is that the low-energy oxygen-protonated urea-H^+ isomer does not react in the simulation time length (2.5 ps), neither to give directly the observed fragments (or other nondetected fragments) nor to isomerize into the nitrogen-protonated structure that can, later, dissociate to the observed ions. For this isomer, we found that single collisions modeled by the simulation often transfer a small amount of vibrational energy, such that OPr → NPr isomerization cannot occur. Furthermore, OPr ions formed with enough energy to isomerize do not on the time scale of the simulations. Of course, in CID experiments multiple collisions can give sufficient energy to OPr molecules for isomerization. Also, if they are only slightly excited above the barrier, they will isomerize if the dynamics is followed for longer times. Then the formed NPr structure can directly dissociate or be further excited by additional collisions, producing the two observed fragments.

This proposed mechanism involving oxygen-to-nitrogen proton transfer before fragmentation was found experimentally in different systems, in particular for proton transfer from a carbonyl site.[55,68−71] This observation led to the "mobile proton model.[72−75]

Another possible source of quantitative discrepancy between experiments and simulations is the different colliding projectile used. Experiments were done using N_2, while simulations were done using Ar for which a classical semiempirical potential was already developed and tested. The differences can come not only from atomic weight differences but also from the rotational and vibrational energy of N_2 that can play a role in ion activation. Our theoretical studies are actually moving in those directions.

Acknowledgment. This work was performed using HPC resources from GENCI-IDRIS (Grant 2009-i2009082123). The contribution of W.L.H. to this project is based upon work supported by the National Science Foundation under Grant No. CHE-0615321 and the Robert A. Welch Foundation under Grant No. D-0005. K.S. acknowledges partial support from Korea National University of Education for research and a sabbatical trip.

References and Notes

(1) Cooks, R. G. In *Collision Spectroscopy*; Cooks, R. G., Ed.; Plenum: New York, 1978.
(2) Fisher, E. R.; Kickel, B. L.; Armentrout, P. B. *J. Phys. Chem.* **1993**, *97*, 10204.
(3) Tosh, R. E.; Shukla, A. K.; Futrell, J. H. *J. Chem. Phys.* **2001**, *114*, 2986.
(4) Muntean, F.; Armentrout, P. B. *J. Chem. Phys.* **2001**, *115*, 1213.
(5) Fu, Y. J.; Laskin, J.; Wang, L. S. *Int. J. Mass Spectrom.* **2006**, *255*, 102.
(6) Carl, D. R.; Moision, R. M.; Armentrout, P. B. *Int. J. Mass Spectrom.* **2007**, *256*, 308.
(7) Armentrout, P. B.; Koizumi, H.; MacKenna, M. *J. Phys. Chem. A* **2005**, *109*, 11365.
(8) Salpin, J.-Y.; Tortajada, J. *J. Mass. Spectrom.* **2002**, *37*, 379.
(9) Hallowita, N.; Carl, D. R.; Armentrout, P. B.; Rodgers, M. T. *J. Phys. Chem. A* **2008**, *112*, 7996.
(10) Chawla, R.; Shukla, A.; Futrell, J. H. *J. Phys. Chem. A* **2001**, *105*, 349.
(11) Buchmann, W.; Spezia, R.; Tournois, G.; Cartailler, T.; Tortajada, J. *J. Mass Spectrom.* **2007**, *42*, 517.
(12) Heaton, A. L.; Armentrout, P. B. *J. Phys. Chem. A* **2008**, *112*, 10156.
(13) Laskin, J.; Denisov, E.; Futrell, J. H. *Int. J. Mass Spectrom.* **2002**, *219*, 189.
(14) Laskin, J.; Denisov, E.; Futrell, J. H. *J. Chem. Phys.* **2002**, *116*, 4302.
(15) Baer, T.; Hase, W. L. *Unimolecular Reaction Dynamics—Theory and Experiments*; Oxford: New York, 1996.
(16) Chesnavich, W. J.; Bowers, M. T. *Gas Phase Ion Chemistry*; Bowers, M. T., Ed.; Academic Press: New York, 1979; Vol. 1, p 119.
(17) Schlag, E. W.; Levine, R. D. *Chem. Phys. Lett.* **1989**, *163*, 523.
(18) Schultz, D. G.; Hanley, L. *J. Chem. Phys.* **1998**, *109*, 10976.
(19) Raz, T.; Levine, R. D. *J. Chem. Phys.* **1996**, *105*, 8097.
(20) Wang, Y.; Hase, W. L.; Song, K. *J. Am. Soc. Mass Spectrom.* **2003**, *14*, 1402.
(21) Burroughs, J. A.; Wainhaus, S. B.; Hanley, L. *J. Chem. Phys.* **1995**, *103*, 6706.
(22) Meroueh, O.; Hase, W. L. *Phys. Chem. Chem. Phys.* **2001**, *3*, 2306.
(23) Meroueh, O.; Song, K.; Hase, W. L. *J. Chem. Phys.* **2003**, *118*, 2893.
(24) Fenn, P. T.; Chen, Y.-J.; Stimson, S.; Ng, C. Y. *J. Phys. Chem. A* **1997**, *101*, 6513.
(25) Martínez-Núñez, E.; Vázquez, S. A.; Marques, J. M. C. *J. Chem. Phys.* **2004**, *121*, 2571.
(26) Chen, Y.-J.; Fenn, P. T.; Lau, K.-C.; Ng, C. Y.; Law, C.-K.; Li, W.-K. *J. Phys. Chem. A* **2002**, *106*, 9729.
(27) Martínez-Núñez, E.; Vázquez, S. A.; Aoiz, E. J.; Castillo, J. F. *J. Phys. Chem. A* **2006**, *110*, 1225.
(28) Martínez-Núñez, E.; Fernández-Ramos, A.; Vázquez, S. A.; Marques, J. M. C.; Xue, M.; Hase, W. L. *J. Chem. Phys.* **2005**, *123*, 154311.
(29) Liu, J.; Song, K.; Hase, W. L.; Anderson, S. L. *J. Chem. Phys.* **2003**, *119*, 3040.
(30) Meroueh, O.; Wang, Y.; Hase, W. L. *J. Phys. Chem. A* **2002**, *106*, 9983.
(31) Lourderaj, U.; Hase, W. L. *J. Phys. Chem. A* **2009**, *113*, 2236.
(32) Sun, L.; Hase, W. L. *Rev. Comput. Chem.* **2003**, *19*, 79.
(33) Peslherbe, G. H.; Wang, H.; Hase, W. L. *Adv. Chem. Phys.* **1999**, *105*, 171.
(34) de Sainte Claire, P.; Hase, W. L. *J. Phys. Chem.* **1996**, *100*, 8190.
(35) Rahaman, A.; Hase, W. L.; Song, K.; Wang, J.; Meroueh, S. O. In *Principles of Mass Spectrometry Applied to Biomolecules*; Laskin, J., Lofshitz, C., Eds.; John Wiley & Sons, Inc.: Hoboken, NJ, 2006.
(36) *Chem. Eng. News* **1987**, *65*, 21.
(37) Raab, W. P. *Cosmet. Toiletries* **1990**, *105*, 97.
(38) March, J. *Advanced Organic Chemistry*, 4th ed.; John Wiley & Sons: New York, 1992.
(39) Rawn, J. D. *Biochemistry*; Carolina Biological Supply Company: Burlington, NC, 1989.
(40) Thomas, G. C.; George, S. *Chem. Rev.* **1997**, *97*, 829.
(41) Franco, L.; Andrei, M.; Andrea, C. *Science* **1994**, *266*, 801.
(42) Lam, P. Y. S.; Jadhav, P. K.; Eyermann, C. J.; Hodge, C. N.; Ru, Y.; Bacheler, L. T.; Meek, J. L.; Otto, M. J.; Rayner, M. M.; Wong, Y. N.; Chang, C.; Weber, P. C.; Jackson, D. A.; Sharpe, T. R.; Erickson-Viitanen, S. *Science* **1994**, *263*, 380.
(43) Corral, I.; Mo, O.; Yanez, M.; Salpin, J.-Y.; Tortajada, J.; Radom, L. *J. Phys. Chem. A* **2004**, *108*, 10080.
(44) Cimas, A.; Gamez, J. A.; Mo, O.; Yanez, M.; Salpin, J.-Y. *Chem. Phys. Lett.* **2008**, *456*, 156.
(45) Rotario, R.; Castano, O.; Herreros, M.; Abboud, J.-L. M. *J. Mol. Struct. (Theochem)* **1996**, *371*, 21.
(46) Wang, F.; Ma, S.; Zhang, D.; Cooks, R. G. *J. Phys. Chem. A* **1998**, *102*, 2988.
(47) Dixon, D. A.; Matsuzawa, N. *J. Phys. Chem.* **1994**, *98*, 3967.
(48) *Gaussian 03*, revision D.01; Frisch, M. J.; et al. Gaussian, Inc.: Wallingford, CT, 2004.
(49) Zhu, L.; Hase, W. L. *QCPE* **1994**, *14*, 644.
(50) Vayner, G.; Addepalli, S. V.; Song, K.; Hase, W. L. *J. Chem. Phys.* **2006**, *125*, 014317.
(51) Meroueh, O.; Hase, W. L. *J. Phys. Chem. A* **1997**, *103*, 3981.
(52) Rogalewicz, F.; Hoppilliard, Y.; Ohanessian, G. *Int. J. Mass Spectrom.* **2001**, *206*, 45.
(53) Salpin, J.-Y.; Guillaumont, S.; Tortajada, J.; MacAleese, L.; Lemaire, J.; Maitre, P. *Chem. Phys. Chem.* **2007**, *8*, 2235.
(54) Bakker, J. M.; Brugnara, M.; Besson, T.; Salpin, J.-Y.; Maitre, P. *J. Phys. Chem. A* **2008**, *112*, 12393.
(55) Tu, Y.-P. *J. Org. Chem.* **2006**, *71*, 5482.
(56) Chapman, S.; Bunker, D. L. *J. Chem. Phys.* **1975**, *62*, 2890.
(57) Sloane, C. S.; Hase, W. L. *J. Chem. Phys.* **1977**, *66*, 1523.
(58) Cho, Y. J.; Vande Linde, S. R.; Zhu, L.; Hase, W. L. *J. Chem. Phys.* **1992**, *96*, 8275.
(59) Hase, W. L.; Duchovic, R. J.; Hu, X.; Komornicki, A.; Lim, K. F.; Lu, D.-h.; Peslherbe, G. H.; Swamy, K. N.; Vande Linde, S. R.; Varandas, A.; Wang, H.; Wolf, R. J. *QCPE* **1996**, *16*, 671.
(60) Hu, X.; Hase, W. L. *J. Comput. Chem.* **1991**, *12*, 1014.
(61) Swope, W. C.; Andersen, H. C.; Berens, P. H.; Wilson, K. R. *J. Chem. Phys.* **1982**, *76*, 637.
(62) Chernushevich, I. V.; Loboda, A. V.; Thomson, B. A. *J. Mass Spectrom* **2001**, *36*, 849.
(63) Salpin, J.-Y. Unpublished results.
(64) de Sainte Claire, P.; Peslherbe, G. H.; Hase, W. L. *J. Phys. Chem.* **1995**, *99*, 8147.
(65) Meroueh, O.; Hase, W. L. *Int. J. Mass Spectrom.* **2000**, *201*, 233.
(66) Park, K.; Song, K.; Hase, W. L. *Int. J. Mass Spectrom.* **2007**, *265*, 326.
(67) Park, K.; Deb, B.; Song, K.; Hase, W. L. *J. Am. Soc. Mass Spectrom.* **2009**, *20*, 939.
(68) Smith, L. R.; Chyall, L. J.; Beasley, B. J.; Kenttamaa, H. I. *J. Am. Chem. Soc.* **1995**, *117*, 7971.
(69) Nold, M. J.; Wesdemiotis, C. *J. Mass Spectrom.* **1996**, *31*, 1169.
(70) Vais, V.; Etinger, A.; Mandelbaum, A. *J. Mass Spectrom.* **1999**, *34*, 755.
(71) Denekamp, C.; Mandelbaum, A. *J. Mass Spectrom.* **2001**, *36*, 422.
(72) Wysocki, V. H.; Tsaprailis, G.; Smith, L. L.; Breci, L. A. *J. Mass Spectrom.* **2000**, *35*, 1399.
(73) Dongré, A. R.; Jones, J. L.; Somogyi, A.; Wysocki, V. H. *J. Am. Chem. Soc.* **1996**, *118*, 8365.
(74) Csonka, I. P.; Paizs, B.; Lendvay, G.; Suhai, S. *Rapid Commun. Mass Spectrom.* **2000**, *14*, 417.
(75) Paizs, B.; Suhai, S. *Mass Spectrom. Rev.* **2005**, *24*, 508.

JP906482V